Journal of Materials Chemistry C

PAPER

View Article Online
View Journal | View Issue

Cite this: J. Mater. Chem. C, 2015, 3, 9095

Synthesis, aggregation-induced emission and electroluminescence properties of a novel compound containing tetraphenylethene, carbazole and dimesitylboron moieties†

Heping Shi,[abc] Zhihua Gong,[a] Dehua Xin,[a] Jesse Roose,[b] Huiren Peng,[d] Shuming Chen,*[d] Jacky W. Y. Lam[b] and Ben Zhong Tang*[bc]

Received 29th June 2015,
Accepted 4th August 2015

DOI: 10.1039/c5tc01928a

www.rsc.org/MaterialsC

In this paper, a new aggregation-induced emission (AIE)-active compound, 1,2-bis(4-(3,6-bis(dimesitylboranyl)-9*H*-carbazol-9-yl)phenyl)-1,2-diphenylethene (**BBDCZPD**), has been successfully synthesized. The building block of **BBDCZPD** comprises tetraphenylethene as the skeleton, carbazole as the hole-transporting moiety and dimesitylboron as the electron-transporting moiety. Its structure is fully characterized using elemental analysis, mass spectrometry and proton nuclear magnetic resonance spectroscopy. The thermal, electrochemical and photophysical properties of **BBDCZPD** are studied using thermal analysis, electrochemical methods, UV-vis absorption spectroscopy and fluorescence spectroscopy, respectively. The results show that **BBDCZPD** exhibits excellent thermal stability and electrochemical stability as well as AIE properties. Moreover, a multilayer organic light-emitting diode (OLED) device is fabricated by using **BBDCZPD** as the non-doped emitter which displays good electroluminescence performances with a turn-on voltage of 5.2 V, a maximum luminance of 5406 cd m^{-2} and a maximum luminance efficiency of 5.34 cd A^{-1}. The electroluminescence properties of **BBDCZPD** demonstrate its potential application in OLEDs.

1. Introduction

Organic light-emitting diodes (OLEDs) have received intensive attention in the scientific community due to their unique advantages of a low driving voltage, high brightness and full-color emission.[1–5] A High-performance electroluminescence (EL) material is the primary factor in enhancing the performance of a OLED device and is helpful to simplify its configuration and lower the construction costs.[6–10] So far, a variety of luminogenic materials have been prepared, but most of these fluorophores usually suffer from aggregation-caused quenching (ACQ).[11] Their good light emissions in solution are weakened greatly in poor solvents or when fabricated as solid thin films owing to the formation of excimers or exciplexes in aggregated states.[12–16] The ACQ effect leads to the unsatisfactory efficiency of organic luminogens in the solid state, thus greatly limiting the scope of the application of such materials as emitting layer materials of OLEDs.[17–20]

In order to alleviate the ACQ effect, scientists have tried numerous methods including chemical, physical and engineering approaches and processes, unfortunately, the results are still far from satisfactory.[21,22] In 2001, Tang *et al.* reported a novel phenomenon: some propeller-like molecules are weakly emissive or non-luminescent in dilute solution but will emit efficiently in the aggregate state. This intriguing phenomenon was named as aggregation induced emission (AIE),[23–27] and is opposite to ACQ. The strong solid state emission of AIE molecules arouses an immense interest from various research groups.[28–31] Many investigations have been rapidly explored in this field to reveal the reaction mechanisms. So far Tang *et al.* have proposed the restriction of the intramolecular rotation (RIR) mechanism.[32] AIE molecules usually contain a structure with molecular rotors, and when fully dissolved, the excited state energy of the molecules is consumed by the rotation of the rotors, the energy is quickly decayed without emission. Upon aggregation, intermolecular interactions between the AIE molecules restrict the rotations of the rotors, causing the molecules to decay *via* radiative channels.[33,34] Based on the RIR mechanism, plenty of new AIE luminogens have been developed and their practical application in OLEDs was explored.[35–41]

[a] School of Chemistry and Chemical Engineering, Shanxi University, Taiyuan 030006, P. R. China. E-mail: hepingshi@sxu.edu.cn
[b] Department of Chemistry, Institute for Advanced Study, Division of Biomedical Engineering, Division of Life Science, State Key Laboratory of Molecular Neuroscience, Institute of Molecular Functional Materials, The Hong Kong University of Science and Technology, Clear Water Bay, Kowloon, Hong Kong, China. E-mail: tangbenz@ust.hk
[c] State Key Laboratory of Luminescent Materials and Devices, South China University of Technology, Guangzhou, Guangdong, 510640, P. R. China
[d] Department of Electrical and Electronic Engineering, South University of Science and Technology of China, Shenzhen, Guangdong, 518055, P. R. China. E-mail: chen.sm@sustc.edu.cn

† Electronic supplementary information (ESI) available. See DOI: 10.1039/c5tc01928a

The tetraphenylethylene (TPE) molecule and its derivatives are among the select class of chromophores which exhibit a remarkable AIE effect.[42–44] They are chosen as great candidates for blue light EL materials owing to their strong blue light emissions, ease of syntheses and simple structures. It has been proved that introducing functional groups as substituents to the TPE molecule is a versatile strategy to obtain luminogens with a good AIE effect and an efficient solid state luminescence. Yuan obtained a novel luminescent TPE derivative, TPEDMesB, through substitutions at the 4-position of the phenyl of TPE with dimesitylboron.[45] The dimesitylboron structure provides good electronic and photophysical properties to the compound. The maximum luminance efficiency of the electroluminescent device with TPEDMesB as the emitting layer is 7.13 cd A^{-1}. Later, Zhao synthesized a group of novel luminescent materials by fusing TPE units and carbazole moieties at the molecular level. The fabricated devices using these compounds as lighting materials show high efficiencies up to 6.3 cd A^{-1} due to the good solid state lighting and hole-transport properties.[46] Recently, Chen synthesized two new TPE derivatives, TPE-NB and TPE-PNPB. The balanced charge-transporting capabilities and the AIE effect of these compounds help to obtain the excellent EL properties of 16.2 cd A^{-1}.[47] The previous work demonstrates that the design and synthesis of TPE derivatives is an efficient way to obtain good EL materials.

Based on the previous work, we synthesized a novel EL compound, 1,2-bis(4-(3,6-bis(dimesitylboranyl)-9*H*-carbazol-9-yl)phenyl)-1,2-diphenylethene (**BBDCZPD**), comprising TPE as the AIE-active moiety, carbazoles as the hole-transporting moieties and dimesitylborons as the electron-transporting moieties. Two carbazole groups were introduced to the 4,4-positions of the 1- and 3-phenyl of TPE and the 3,6-positions of each carbazole group were linked to two dimesitylborons. The synthetic route is summarized in Scheme 1. The chemical structure of **BBDCZPD** was fully characterized using proton nuclear magnetic resonance (^{1}H NMR) spectroscopy, ^{13}carbon (^{13}C NMR) spectroscopy, mass spectrometry (MS) and elemental analysis. The thermal, electrochemical, photoluminescence (PL) and EL properties of **BBDCZPD** are studied in detail.

2. Experimental

All reagents were used as received from commercial sources without further purification unless otherwise stated. Solvents were freshly distilled according to the standard procedures. Tetrahydrofuran (THF) was refluxed with sodium and benzophenone, and freshly distilled prior to use. All reactions were carried out under a nitrogen atmosphere by using Schlenk techniques.

2.1. Synthesis of 1,2-bis(4-(3,6-bis(dimesitylboryl)-9*H*-carbazol-9-yl)phenyl)-1,2-diphenylethene (BBDCZPD)

2.1.1. Synthesis of 4-(9*H*-carbazol-9-yl)phenyl)(phenyl)-methanone (1). Into a stirred mixture of 4-bromobenzophenone (5.01 g, 30 mmol), carbazole (8.613 g, 33 mmol) and toluene (120 mL), $Pd(OAc)_2$ (0.336 g, 1.5 mmol), P(*t*-Bu)$_3$ (3.0 mL, 3.0 mmol) and K_2CO_3 (120 mmol, 16.58 g) were slowly added under nitrogen. The mixture was heated at 120 °C for 48 h. After being cooled to room temperature, cold water (600 mL) was added to the mixture. The organic layer was extracted with dichloromethane, and washed with water and diluted hydrochloric acid. The crude product was purified by silica-gel chromatography (1 : 1 dichloromethane : petroleum ether) to give a gray solid (76.9%, 8.0 g): ^{1}H NMR (600 MHz, $CDCl_3$) δ (ppm): 8.19–8.17 (d, J = 7.10 Hz, 2H), 8.11–8.09 (d, J = 8.10 Hz, 2H), 7.93–7.91 (d, J = 6.40 Hz, 2H), 7.77–7.74 (d, J = 6.50 Hz, 2H), 7.64 (t, J = 6.80 Hz, 1H), 7.62–7.55 (d, J = 7.30 Hz, 4H), 7.49–7.47 (t, J = 6.40 Hz, 2H), 7.38–7.36 (t, J = 6.90 Hz, 2H).

2.1.2. Synthesis of 4-(3,6-dibromo-9*H*-carbazol-9-yl)phenyl-(phenyl)methanone (2). *N*-Bromosuccinimide (3.916 g NBS, 22.0 mmol) in dimethylformamide (40 mL, DMF) was added

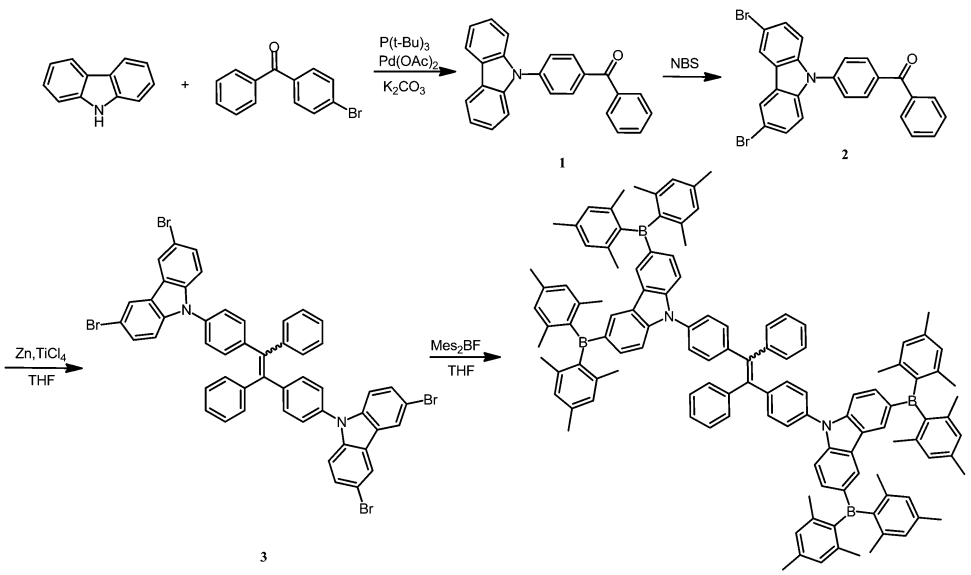

Scheme 1 Synthetic route of **BBDCZPD**.

dropwise to a solution of **1** (6.941 g, 20.0 mmol) in DMF (20 mL) at 0 °C. The mixture was stirred for 12 h at room temperature. Then, ice water was added to the mixture and the white precipitate was collected by filtration to afford **2** (8.585 g, 85%): ^{1}H NMR (600 MHz, $CDCl_3$) δ (ppm): 8.22 (d, J = 1.80 Hz, 2H), 8.09–8.06 (t, J = 8.40 Hz, 2H), 7.92–7.88 (m, 2H), 7.70–7.67 (m, 3H), 7.58–7.52 (m, 4H), 7.38 (d, J = 8.73 Hz, 2H).

2.1.3. Synthesis of 1,2-bis(4-(3,6-dibromo-9*H*-carbazol-9-yl)phenyl-1,2-diphenylethene (3). To a 250 mL flask equipped with a stirrer zinc powder (4.628 g, 71.2 mmol) and 150 mL of THF were added. $TiCl_4$ (4.0 mL, 40 mmol) was slowly added by a syringe at −78 °C under nitrogen. The mixture was returned to room temperature and then heated to reflux for 4 h. After being cooled to room temperature, **2** (4.5 g, 8.9 mmol) in 40 mL of THF solution was added to the mixture. The resulting mixture was heated at 70 °C overnight. Then, the reaction was quenched with 10% K_2CO_3 aqueous solution and extracted with dichloromethane. The organic layer was collected and concentrated. The crude product was purified by silica-gel chromatography (1 : 1 dichloromethane : petroleum ether) to give a yellow-green solid (3.3 g, 37.9%): ^{1}H NMR (600 MHz, $CDCl_3$) δ (ppm): 8.16–8.14 (d, J = 7.82 Hz, 4H), 7.50–7.44 (m, 5H), 7.43–7.39 (m, 6H), 7.38–7.27 (m, 10H), 7.26–7.20 (m, 5H). ^{13}C NMR (600 MHz, $CDCl_3$) δ (ppm): 143.56, 143.13, 141.92, 141.25, 139.49, 137.55, 134.10, 132.14, 130.46, 127.92, 127.67, 127.43, 127.10, 126.50, 126.10, 125.54, 123.23, 122.13, 112.45. MS: m/z 978.2131.

2.1.4. Synthesis of 1,2-bis(4-(3,6-bis(dimesitylboryl)-9*H*-carbazol-9-yl)phenyl)-1,2-diphenylethene (BBDCZPD). Into a 100 mL round-bottom flask**3** (1.0 g, 1.0 mmol) was placed. The flask was evacuated under vacuum and flushed with dry nitrogen three times. Then, 80 mL of dry THF was added. The mixture was cooled to −78 °C and 6.15 mL (1.3 M in hexane, 8 mmol) of *t*-BuLi was added dropwise using a syringe. The mixture was stirred for 4 h at −78 °C, and then dimesitylboron fluoride (2.35 g, 8.8 mmol) was slowly added to the reaction solution. The mixture was warmed slowly to room temperature and stirred for 24 h. Then, the mixture was quenched with ice water (200 mL) and stirred for 2 h. The organic layer was extracted with dichloromethane and the combined organic extracts were dried over anhydrous $MgSO_4$. After filtration and solvent evaporation, the crude product was purified by silica gel column chromatography (1 : 1 dichloromethane : petroleum ether). A light blue solid of **BBDCZPD** was obtained (0.50 g, 31.2%): ^{1}H NMR (600 MHz, $CDCl_3$) δ (ppm): 8.36–8.29 (d, J = 3.57 Hz, 4H), 7.58–7.53 (d, J = 7.36 Hz, 4H), 7.41–7.37 (d, J = 7.10 Hz, 2H), 7.36–7.31 (m, 5H), 7.31–7.27 (m, 4H), 7.25–7.24 (s, 1H), 7.23–7.10 (m, 10H), 6.87–6.77 (d, 16H), 2.35–2.27 (d, 24H), 2.07–1.94 (t, 48H). ^{13}C NMR (600 MHz, $CDCl_3$) δ (ppm): 146.411, 144.980, 143.911, 143.136, 142.898, 141.067, 140.929, 138.194, 135.853, 134.300, 134.293, 134.212, 131.156, 131.078, 130.821, 130.804, 130.765, 130.691, 129.714, 129.987, 129.328, 128.965, 128.512, 126.324, 125.787, 125.345, 123.343, 122.965, 113.987, 112.914, and 112.109. MS: m/z 1655.1232 anal. calcd for $C_{122}H_{118}B_4N_2$: C 88.51%, H 7.18% and N 1.69%. Found: C 88.72%, H 7.10%, and N 1.62%.

2.2. Measurements and characterization

All NMR spectra were measured on a Bruker 600 MHz spectrometer. Thermogravimetric analysis (TGA) was performed on a TGA 2050 thermogravimetric analyzer under a N_2 atmosphere with a heating rate of 10 °C min^{-1} from room temperature to 750 °C. Differential scanning calorimetry (DSC) was performed using a Q2000 DSC differential scanning calorimeter under a N_2 atmosphere with a heating rate of 10 °C min^{-1} from room temperature to 250 °C. Elemental analyses were performed on an Element Analysis System. Mass spectra were recorded with an LC-MS system consisting of a Waters 1525 pump and a Micromass ZQ4000 single quadrupole mass spectrometer detector. Cyclic voltammetry (CV) was performed on a CHI-600C electrochemical analyzer. The CV measurements were carried out with a conventional three-electrode configuration consisting of a glassy carbon working electrode, a platinum-disk auxiliary electrode and an Ag/AgCl reference electrode, and the scan speed was 50 mV s^{-1}. UV-vis absorption spectra were acquired using a Shimadzu UV-2450 absorption spectrophotometer. Fluorescence spectra were obtained using a Hitachi F-4500 spectrofluorometer. The fluorescence quantum yield was determined using quinine sulfate as the reference (excited at 350 nm). All measurements were performed at room temperature.

2.3. Device fabrication and measurement

The multilayer OLEDs were fabricated by a vacuum-deposition method. Organic layers were fabricated by high-vacuum (5×10^{-4} Pa) thermal evaporation onto a glass (3 cm × 3 cm) substrate precoated with an ITO layer. Dipyrazinoquinoxaline-2,3,6,7,10,11-hexacarbonitrile (HATCN) was used as the hole injection layer, *N*,*N*-bis(naphthalene)-*N*,*N*-bis(phenyl)benzidine (NPB) was used as the hole-transport layer (HTL), **BBDCZPD** was used as the emitting layer, 1,3,5-tri(1-phenyl-1*H*-benzo[*d*]imidazol-2-yl)phenyl (TPBi) was used as the electron-transport layer (ETL) and LiF/Al was evaporated as the cathode. All organic layers were sequentially deposited. Thermal deposition rates for organic materials, LiF and Al were 0.5 A s^{-1}, 0.5 A s^{-1} and 1 A s^{-1}, respectively. The active area of the devices is 9.0 mm^2. The EL spectra were measured on a Hitachi MPF-4 fluorescence spectrometer. The voltage current density characteristics of OLEDs were recorded on a Keithley 2400 Source Meter. The current density–voltage–luminance curves were measured with a 3645 DC power supply combined with a 1980A spot photometer and were recorded simultaneously. All measurements were done at room temperature.

3. Results and discussion

3.1. Synthesis of BBDCZPD

Scheme 1 displays that compound **1** was obtained by the modified Ullman coupling reaction between carbazole and 4-bromobenzophenone. Then, compound **2** was prepared by bromination of **1** with NBS. Compound **3** was produced with a high yield by a McMurry coupling reaction in the Zn/$TiCl_4$ catalytic system. The final product **BBDCZPD** was obtained by

Table 1 Physical properties of **BBDCZPD**

Com.	λ_{abs} [a] (nm)	λ_{em} [b] (nm)	λ_{em} [c] (nm)	Φ [d]	T_d [e] (°C)	T_g [e] (°C)	HOMO/LUMO [f] (eV)	E_g [g] (eV)	HOMO/LUMO [h] (eV)	E_g [h] (eV)
BBDCZPD	318/362	470	468	0.46	219	100	−5.26/−2.08	3.18	−5.42/−1.74	3.68

[a] Measured in THF. [b] Measured in THF + H_2O (1 : 9). [c] Measured in film. [d] Measured in solid. [e] Obtained from TGA and DSC. [f] Obtained from CV in CH_3CN/*n*-Bu_4NClO_4 and estimated from HOMO = $-(4.4 + E^{ox}_{onset})$; LUMO = HOMO + E_g. [g] Calculated from the absorption edge, $E_g = 1240/\lambda_{onset}$. [h] Obtained from DFT calculations.

reacting **3** with *t*-BuLi, followed by the addition of dimesitylboron fluoride. All of the intermediates and the final compound were purified by column chromatography on silica gel using petroleum ether and dichloromethane as eluents and were fully characterized using ^{1}H NMR and ^{13}C NMR, MS and elemental analysis.

3.2. Thermal properties

The thermal properties of **BBDCZPD** were characterized using TGA and DSC under a nitrogen atmosphere as shown in Fig. S1 and S2 (ESI†). The decomposition temperature (T_d) corresponding to a 5.0% weight loss of **BBDCZPD** is 219 °C and the glass transition temperature (T_g) is 100 °C. These data are collected in Table 1. The high T_d might be attributed to its large molecular mass. The high T_g should be ascribed to the introduction of rigid carbazole moieties. The high T_d and T_g indicate that **BBDCZPD** has excellent thermal and morphological stability which can contribute to the preparation of the homogeneous and stable amorphous emissive layer in OLED devices.

3.3. Photophysical properties of BBDCZPD

The UV-vis absorption spectra of **BBDCZPD** were measured in different solvents (10 μM) and are shown in Fig. S3 (ESI†). Two main bands at 290–330 and 330–400 nm are observed which are almost the same in different polar solvents, inferring the independence of the UV-vis absorption to the solvent polarity. The high energy absorption band at 290–330 nm is attributed to the π–π* electronic transitions of the skeleton of **BBDCZPD** and the low energy absorption band at 330–400 nm is assigned to an intramolecular charge transfer (ICT) band from the carbazole moieties (as electron-donors) to the TPE moiety and dimesitylboron moieties (as electron-acceptors) of **BBDCZPD**. Moreover, the optical energy band gap calculated from the absorption band edges of the UV-vis absorption spectra is approximately 3.18 eV. The relevant data are collected in Table 1.

The fluorescence spectra of **BBDCZPD** were measured in different solvents (10 μM) and are shown in Fig. S4 (ESI†). **BBDCZPD** exhibits weak emissions in various solvents and the emission spectra consist of one broad band in various solvents except *n*-hexane. When the polarity of the solvent increases, a bathochromic shift of 38 nm ranging from 374 nm (in *n*-hexane) to 412 nm (in DMSO) is observed. Such a distinct solvatochromism indicates that ICT takes place during the excitation process. In THF, the emission peak at 392 nm can be ascribed to the twisted intramolecular transfer (TICT) emission because of the twisted molecular structure and the push–pull electronic effect. The emission peak at 490 nm is assigned to the ICT emission from the carbazole moieties to the TPE unit. We infer that the introduction of the bulky dimesitylboron moieties partly impedes the intramolecular rotation of the TPE units, resulting in light emission in solution, which is different from the conventional AIE effect. It is noteworthy that only a weak signal centered at 490 nm is recorded, indicating the effective quenching of the ICT emission from carbazole to TPE. The solid emission spectrum of **BBDCZPD** is obtained by measuring its film as depicted in Fig. S5 (ESI†). The spectrum shows the emission maximum at 468 nm. The data is collected in Table 1. The solid absolute fluorescence yield (Φ_s = 0.46) of **BBDCZPD** was measured using the integrating sphere method and its data is also collected in Table 1. The PL properties of **BBDCZPD** in the film indicate that it could be used as an optoelectronic material with blue light emission in OLEDs.

3.4. AIE behavior of BBDCZPD

The AIE behavior of compounds with a TPE moiety has been largely reported in the literature. It is expected that **BBDCZPD** is also an AIE-active luminogen since TPE is an archetype AIE luminogen. To determine the AIE characteristics of **BBDCZPD**, the change in the PL intensity with various various water content of THF–water solvent mixtures was monitored. Here, THF acts as the solvent and water acts as the non-solvent. Fig. 1(a) displays the PL spectra of **BBDCZPD** in THF–water solvent mixtures containing different water fractions (f_w) at an excitation wavelength of 350 nm. **BBDCZPD** displays a very weak PL emission in pure THF (Fig. S4, ESI†). When **BBDCZPD** is molecularly dissolved in aqueous mixtures with $f_w < 50\%$, the solutions show barely discernible emissions with a fluorescence quantum yield (ϕ) of 0.38% (the PL peak is at 390 nm). When more water is added ($f_w > 50\%$), the solvating power of the mixture is worsened to such an extent that nanoparticles begin to form and the purple emission band centered at 390 nm gradually ''turns-off'', along with a blue emission band at 485 nm rapidly ''turning-on''. It is suggested that the aggregation of molecules causes the quenching of the fluorescence emission at 390 nm and the emergence of fluorescence emission at 485 nm. This is due to the restrictions of the intramolecular rotations of the TPE unit, resulting in AIE. A higher water content populates the aggregates, thereby boosting its light emission to a greater extent. In the f_w = 70% aqueous mixture, the peak wavelength is blue-shifted to 478 nm, which may be attributed to the fact that the less polar environment inside the nanoparticles alleviates the CT effect. When f_w is higher than 80%, a small increase in f_w can promote a large increase in the PL intensity. When f_w is 95%, the PL intensity reaches a maximum at 470 nm and ϕ increases to 58% (Table 1). Fig. 1(b) depicts the plot of $[(I/I_0) - 1]$ against f_w, where I_0 and I are the PL intensities

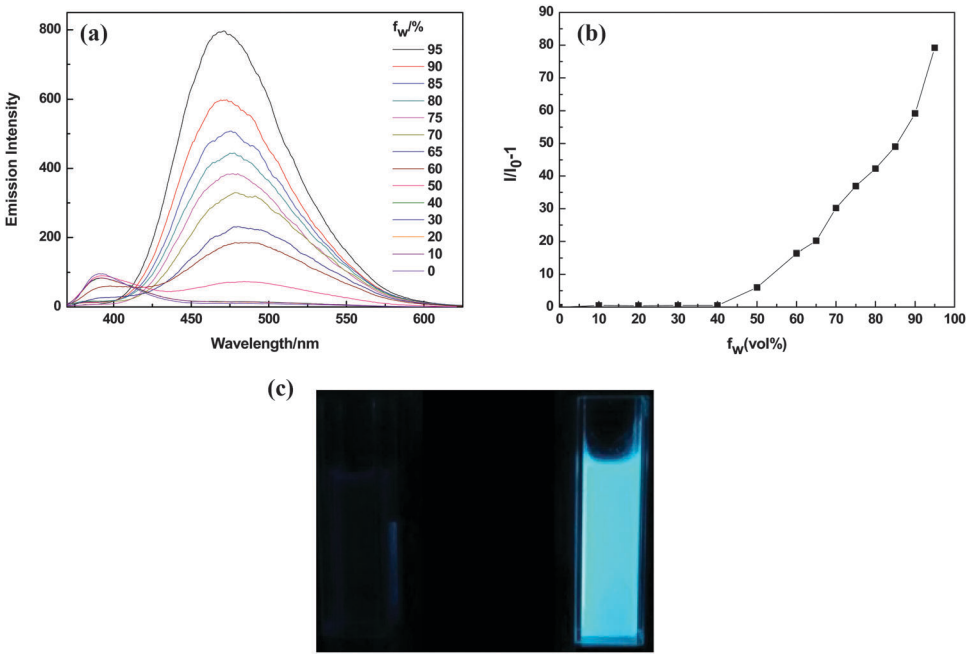

Fig. 1 (a) PL spectra of **BBDCZPD** in THF–water mixtures with various water content (excited at 350 nm). (b) Plot of $(I/I_0) - 1$ against water volume fraction (f_w), where I_0 and I are the PL intensities without and with water in the THF–water mixtures. (c) Photographic images of **BBDCZPD** in a THF–water mixture of f_w (i) 0.0 and (ii) 95%.

without and with water in the THF–water mixture. The fluorescence intensity increases *ca.* 120-fold in f_w, 95% when compared to that of THF. The ϕ increases *ca.* 150-fold. Fig. 1(c) displays the photographic images of **BBDCZPD** in the THF–water mixture of f_w 0.0 and 95%, respectively. They clearly show the change from the non-emissive to the strong blue emissive nature of the molecular species of **BBDCZPD**. It is obvious that water could induce the PL of **BBDCZPD** in a THF–water solvent mixture, attributed to the AIE of **BBDCZPD** in a high water content solvent mixture. These results strongly indicate the prominent aggregation induced emission (AIE) characteristics of **BBDCZPD**, attributed to the RIR process in the aggregate formation which populates the radioactive decay of the excitons and makes the luminogen fluorescence strong.

3.5. Theoretical calculation

To gain a deep insight into the optical behaviors of **BBDCZPD**, its geometrical and electronic properties were optimized at the B3LYP level with the 6-31G(d,p) basis set using the Gaussian 03 program package.[48–51] Fig. 2 shows the optimal structures and the highest occupied molecular orbital (HOMO) and lowest unoccupied molecular orbital (LUMO) orbital distributions. The TPE unit is twisted from the plane of the carbazole and the peripheral dimesitylboron moieties forming propeller-like conformations originating from their trigonal boron centers. The twisted conformation will prevent emission quenching caused by the unfavorable π–π* stacking interaction. The HOMO and LUMO distributions are dominated by the central TPE unit and carbazole moieties. The electron density of the HOMO is localized on the TPE core and carbazole units while the electron density of the LUMO is localized mainly on the TPE

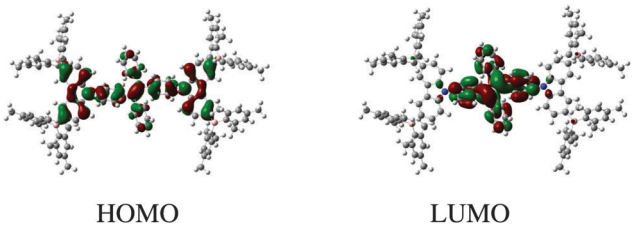

Fig. 2 The optimal structure and HOMO and LUMO distributions of **BBDCZPD**.

core. However, the dimesitylboron units have almost no contribution to the HOMO and LUMO, manifesting an inward ICT from the carbazole moieties to the TPE core. The calculated HOMO energy level, LUMO energy level and energy gap are −5.42, −1.74 and 3.68 eV, respectively. The calculated value is somewhat higher than the experimental value (Table 1).

3.6. Electrochemical properties

The electrochemical properties of **BBDCZPD** were studied using cyclic voltammetry (CV) with Ag/AgCl as the reference electrode. The measurements were conducted on 1.0 mM **BBDCZPD** in acetonitrile containing 0.10 M tetrabutylammonium perchlorate as the supporting electrolyte under a nitrogen atmosphere as shown in Fig. S6 (ESI†). Two reversible oxidation peaks and two reversible reduction peaks are observed within the entire electrochemical window of acetonitrile. The reversible oxidation peaks at around 0.86 and 1.21 V are assigned to the oxidation of carbazole and tetraphenylethene, respectively. The reversible reduction peak at around −0.65 and −1.81 V are attributed to the reduction of tetraphenylethene and dimesitylborons, respectively.

The HOMO energy level can be calculated with the empirical equation: HOMO = $-(E_{ox} + 4.40)$ eV, where E_{ox} is the onset oxidation potential.[52] The E_{ox} of **BBDCZPD** is 0.86 V and the HOMO energy level of **BBDCZPD** is 5.26 eV. The E_g is estimated to be 3.18 eV using the absorption edge of the absorption spectrum of **BBDCZPD.** The LUMO energy level of **BBDCZPD** is thus 2.08 eV which is calculated from the HOMO energy level and E_g. The HOMO, LUMO and E_g of **BBDCZPD** are very close to the theoretical values (Table 1). The HOMO level of **BBDCZPD** matches well with those of two common hole-transporting materials, *N*,*N*′-bis-(1-naphthalenyl)-*N*,*N*′-bis-phenyl-(1,1′-biphenyl)-4,4′-diamine (5.4 eV)[53] and 4,4′-cyclohexylidenebis[*N*,*N*-bis(4-methylphenyl)benzenamine] (5.5 eV),[54] indicating that **BBDCZPD** can be used as an effective hole-transporting material for OLEDs. Similarly, the LUMO level of **BBDCZPD** also matches well with those of two common electron-transporting materials, 1,3,5-tris(1-phenyl-1*H*-benzimidazol-2-yl)benzene (2.39 eV) and 2,9-dimethyl-4,7-diphenyl-1,10-phenanthroline (2.44 eV). The barrier to electron transport from the electron-transporting layer to the emitting layer is quite small, which is beneficial for use as electron-transporting materials for OLEDs. Furthermore, the CV curves of the compound remained unchanged after multiple successive potential scans, indicating that the compound has excellent redox properties.[55]

3.7. Electroluminescence

In order to evaluate **BBDCZPD** as a potential luminescent material for its application in OLEDs, multilayer non-doped OLEDs with a configuration of ITO/HATCN (40 nm)/NPB (40 nm)/**BBDCZPD** (20 nm)/TPBI (40 nm)/LiF (1 nm)/Al (80 nm) were fabricated using **BBDCZPD** as the light emitter. *N*,*N*-Bis(1-naphthyl)-*N*,*N*-diphenyl-benzidine (NPB) and 2,2′,2″-(1,3,5-benzinetriyl)tris(1-phenyl-1*H*-benzimidazole) (TPBI) were adopted as the hole-transporting and electron-transporting layers, respectively, HATCN serves as the hole-injecting layer. The electroluminescence spectrum of Device A is displayed in Fig. S7 (ESI†), showing that **BBDCZPD** emits a bluish green light (peak maximum, λ_{max} 493 nm) with a Commission International d'Eclairage (CIE) chromaticity coordinate of (0.19, 0.34), which is red-shifted about 25 nm in contrast with its PL emission in solid film (λ_{max} 468 nm). The current efficiency–current density and the current density–voltage–luminance curves of Device A are depicted in Fig. 3 and 4, respectively. The current efficiency–voltage curve of Device A is shown in Fig. S8 (ESI†). The electroluminescence data for Device A are summarized in Table 2. The turn-on voltage, maximum luminance and maximum luminance efficiency of Device A are 5.2 V, 5406 cd m^{-2} (at 15 V) and 5.34 cd A^{-1} (at 8.2 V), respectively. It should be pointed out that the EL performances were obtained in a non-optimized test device under ordinary laboratory conditions. The device performances may be further improved by an optimization of the layer thicknesses and processing conditions. Studies on the improvement of the device performances are currently underway.

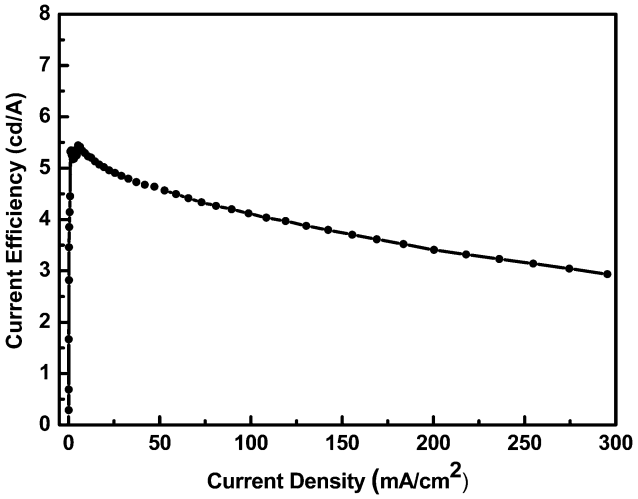

Fig. 3 Current efficiency–current density curve of Device A.

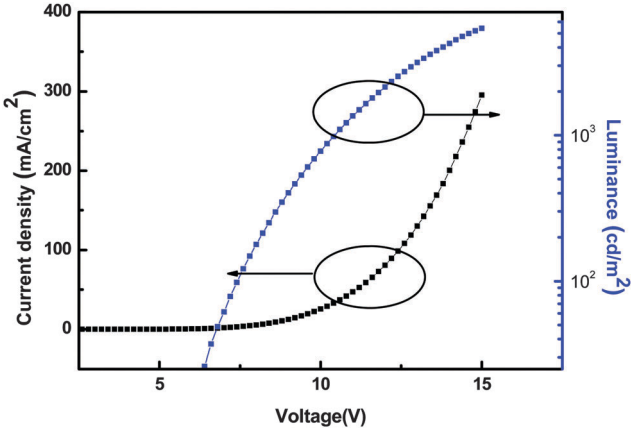

Fig. 4 Current density–voltage–luminance curves of Device A.

Table 2 Electroluminescence characteristics of Device A.[a]

Device	λ_{el} (nm)	V_{on} (V)	L_{max} (cd m^{-2})	$\eta_{L,max}$ (cd A^{-1})
Device A	493	5.2	5406	5.34

[a] V_{on} = turn-on voltage at 1 cd m^{-2}, L_{max} = maximum luminance, $\eta_{L,max}$ = maximum luminance efficiency.

4. Conclusion

In summary, a new AIE-active compound (**BBDCZPD**) is successfully synthesized by combining tetraphenylethene as the skeleton, carbazole as the hole-transporting moiety and dimesitylborons as the electron-transporting moiety. The structure and properties of **BBDCZPD** were fully characterized by experimental and theoretical methods. Our results demonstrate that **BBDCZPD** has excellent thermal stability (T_d = 219 °C) and electrochemical stability as well as AIE properties. Moreover, a multilayer organic light-emitting diode device was fabricated by using **BBDCZPD** as the non-doped emitter. The device shows a bluish green light emitting at a peak maximum of 493 nm with a CIE coordinate of (0.19, 0.34) and good performances with a turn-on voltage of 5.2 V, a maximum luminance of 5406 cd m^{-2} and a maximum

luminance efficiency of 5.34 cd A^{-1}. All results indicate that **BBDCZPD** is a promising material for the construction for efficient non-doped blue OLEDs. Our work provides a new strategy of developing highly efficient EL materials.

Acknowledgements

This work was supported by the Natural Science Foundation of Shanxi Province (No. 2013011013-1); Beijing National Laboratory for Molecular Sciences (No. BNLMS 2013031); Open Fund of the State Key Laboratory of Luminescent Materials and Devices, South China University of Technology (No. 2014-skllmd-09); Scientific and Technological Innovation Programs of Higher Education Institutions in Shanxi Province (No. 2014109 and 2012005); National Natural Science Foundation of China (No. 61405089); The Innovation of Science and Technology Committee of Shenzhen (No. JCYJ20140417105742713). State Key Laboratory of Structural Chemistry, Fujian Institute of Research on the Structure of Matter, Chinese Academy of Sciences (No. 20140016) and Fund of Key Laboratory of Optoelectronic Materials Chemistry and Physics, Chinese Academy of Sciences (No. 2008DP173016). The authors express their sincere thanks to the Advanced Computing Facilities of the Supercomputing Centre of Computer Network Information Centre of Chinese Academy of Sciences for all the theoretical calculations.

References

1 C. W. Tang and S. A. VanSlyke, *Appl. Phys. Lett.*, 1987, **51**, 913–915.
2 C. Adachi, M. A. Baldo and S. R. Forrest, *J. Appl. Phys.*, 2000, **87**, 8049–8055.
3 X. T. Tao, H. Suzuki, T. Wada, H. Suzuki and S. Miyata, *Appl. Phys. Lett.*, 1999, **75**, 1655–1657.
4 J. H. Burroughes, D. D. C. Bradley, A. R. Brown, R. N. Marks, K. Mackay, R. H. Friend, P. L. Burns and A. B. Holmes, *Nature*, 1990, **347**, 539–541.
5 L. S. Hung and C. H. Chen, *Mater. Sci. Eng., R*, 2002, **39**, 143–222.
6 J. Li, C. Ma, J. Tang, C. S. Lee and S. Lee, *Chem. Mater.*, 2005, **17**, 615–619.
7 J. Li, D. Liu, Y. Li, C. S. Lee, H. Kwong and S. Lee, *Chem. Mater.*, 2005, **17**, 1208–1212.
8 D. Braun and A. J. Heeger, *Appl. Phys. Lett.*, 1991, **58**, 1982–1984.
9 W. S. Wu, M. Inbasekaran, M. Hudack, D. Welsh, W. L. Yu, Y. Cheng, C. Wang, S. Kram, M. Tacey, M. Bernius, R. Fletcher, K. Kiszka, S. Munger and J. O'Brien, *Microelectron. J.*, 2004, **35**, 343–348.
10 M. T. Bernius, M. Inbasekaran, J. J. O'Brien and W. Wu, *Adv. Mater.*, 2000, **12**, 1737–1749.
11 X. Cheng, H. Y. Zhang, K. Q. Ye, H. Y. Zhang and Y. Wang, *J. Mater. Chem. C*, 2013, **1**, 7507–7512.
12 M. Belletete, J. Bouchard, M. Leclerc and G. Durocher, *Macromolecules*, 2005, **38**, 880–887.
13 R. Jakubiak, C. J. Collison, W. C. Wan and L. Rothberg, *J. Phys. Chem. A*, 1999, **103**, 2394–2398.
14 A. Menon, M. Galvin, K. A. Walz and L. Rothberg, *Synth. Met.*, 2004, **141**, 197–202.
15 C.-T. Chen, *Chem. Mater.*, 2004, **16**, 4389–4400.
16 M. Grell, D. D. C. Bradley, G. Ungar, J. Hill and K. S. Whitehead, *Macromolecules*, 1999, **32**, 5810–5817.
17 B. J. Xu, Z. G. Chi, H. Y. Li, X. Q. Zhang, X. F. Li, S. W. Liu, Y. Zhang and J. R. Xu, *J. Phys. Chem. C*, 2011, **115**, 17574–17581.
18 B. W. D'Andrade and S. R. Forrest, *Adv. Mater.*, 2004, **16**, 1585–1595.
19 T. Y. Han, X. Feng, B. Tong, J. B. Shi, L. Chen, J. G. Zhi and Y. P. Dong, *Chem. Commun.*, 2012, **48**, 416–418.
20 X. Y. Liu, D. R. Bai and S. Wang, *Angew. Chem.*, 2006, **118**, 5601–5604.
21 A. C. Grimsdale, K. L. Chan, R. E. Martin, P. G. Jokisz and A. B. Holmes, *Chem. Rev.*, 2009, **109**, 897–1091.
22 J. Liu, J. W. Y. Lam and B. Z. Tang, *Chem. Rev.*, 2009, **109**, 5799–5867.
23 J. W. Chen, C. C. W. Law, J. W. Y. Lam, Y. P. Dong, S. M. F. Lo, I. D. Williams, D. B. Zhu and B. Z. Tang, *Chem. Mater.*, 2003, **15**, 1535–1546.
24 J. Huang, Y. B. Jiang, J. Yang, R. L. Tang, N. Xie, Q. Q. Li, H. S. Kwok, B. Z. Tang and Z. Li, *J. Mater. Chem. C*, 2014, **2**, 2028–2036.
25 C. Liu, H. Y. Luo, G. Shi, J. J. Yang, Z. G. Chi and Y. G. Ma, *J. Mater. Chem. C*, 2015, **3**, 3752–3759.
26 L. F. Zhao, Y. L. Lin, T. Liu, H. X. Li, Y. Xiong, W. Z. Yuan, H. H.-Y. Sung, I. D. Williams, Y. M. Zhang and B. Z. Tang, *J. Mater. Chem. C*, 2015, **3**, 4903–4909.
27 Y. Y. Gong, J. Liu, Y. R. Zhang, G. F. He, Y. Lu, W. B. Fan, W. Z. Yuan, J. Z. Sun and Y. M. Zhang, *J. Mater. Chem. C*, 2014, **2**, 7552–7560.
28 J. W. Chen, B. Xu, X. Y. Ouyang, B. Z. Tang and Y. Cao, *J. Phys. Chem. A*, 2004, **108**, 7522–7526.
29 Y. Ren, J. W. Y. Lam, Y. Q. Dong, B. Z. Tang and K. S. Wong, *J. Phys. Chem. B*, 2005, **109**, 1135–1140.
30 Z. X. Wang, H. X. Shao, J. C. Ye, L. Tang and P. Lu, *J. Phys. Chem. B*, 2005, **109**, 19627–19633.
31 G. F. Zhang, Z. Q. Chen, M. P. Aldred, Z. Hu, T. Chen, Z. L. Huang, X. G. Meng and M. Q. Zhu, *Chem. Commun.*, 2014, **50**, 12058–12060.
32 Y. N. Hong, J. W. Y Lam and B. Z. Tang, *Chem. Soc. Rev.*, 2011, **40**, 5361–5388.
33 S. Zhang, A. J. Qin, J. Z. Sun and B. Z. Tang, *Prog. Chem.*, 2011, **23**, 623–636.
34 J. Z. Liu, J. W. Y. Lam and B. Z. Tang, *J. Inorg. Organomet. Polym.*, 2009, **19**, 249–285.
35 W. B. Wu, S. H. Ye, R. L. Tang, L. J. Huang, Q. Q. Li, G. Yu, Y. Q. Liu, J. G. Qin and Z. Li, *Polymer*, 2012, **53**, 3163–3171.
36 W. L. Gong, B. Wang, M. P. Aldred, C. Li, G. F. Zhang, T. Chen, L. Wang and M. Q. Zhu, *J. Mater. Chem. C*, 2014, **2**, 7001–7012.
37 X. Y. Tang, L. Yao, H. Liu, F. Z. Shen, S. T. Zhang, H. H. Zhang, P. Lu and Y. G. Ma, *Chem. – Eur. J.*, 2014, **20**, 7589–7592.

38 J. Huang, X. Yang, X. J. Li, P. Y. Chen, R. L. Tang, F. Li, P. Lu, Y. G. Ma, L. Wang, J. G. Qin, Q. Q. Li and Z. Li, *Chem. Commun.*, 2012, **48**, 9586–9588.
39 M. P. Aldred, G. F. Zhang, C. Li, G. Chen, T. Chen and M. Q. Zhu, *J. Mater. Chem. C*, 2013, **1**, 6709–6718.
40 A. J. Qin, J. W. Y. Lam and B. Z. Tang, *Chem. Soc. Rev.*, 2010, **39**, 2522–2544.
41 Y. N. Hong, J. W. Y. Lam and B. Z. Tang, *Chem. Commun.*, 2009, 4332–4353.
42 M. P. Aldred, C. Li, G. F Zhang, W. L. Gong, A. D. Q. Li, Y. F. Dai, D. G. Ma and M. Q. Zhu, *J. Mater. Chem.*, 2012, **22**, 7515–7528.
43 G. F. Zhang, M. P. Aldred, W. L. Gong, C. Li and M. Q. Zhu, *Chem. Commun.*, 2012, **48**, 7711–7713.
44 C. Li, W. L. Gong, Z. Hu, M. P. Aldred, G. F. Zhang, T. Chen, Z. L. Huang and M. Q. Zhu, *RSC Adv.*, 2013, **3**, 8967–8972.
45 W. Z. Yuan, S. M. Chen, J. W. Y. Lam, C. M. Deng, P. Lu, H. H. Y. Sung, I. D. Williams, H. S. Kwok, Y. M. Zhang and B. Z. Tang, *Chem. Commun.*, 2011, **47**, 11216–11218.
46 Z. J. Zhao, P. Lu, J. W. Y. Lam, Z. M. Wang, C. Y. K. Chan, H. H. Y. Sung, I. D. Williams, Y. G. Ma and B. Z. Tang, *Chem. Sci.*, 2011, **2**, 672–675.
47 L. Chen, Y. B. Jiang, H. Nie, R. R. Hu, H. S. Kwok, F. Huang, A. J. Qin, Z. J. Zhao and B. Z. Tang, *ACS Appl. Mater. Interfaces*, 2014, **6**, 17215–17225.
48 P. Hohenberg and W. Kohn, *Phys. Rev. B: Solid State*, 1964, **136**, 864–871.
49 W. Kohn and L. J. Sham, *Phys. Rev. A: At., Mol., Opt. Phys.*, 1965, **140**, 1133–1138.
50 J. B. Foresman, M. H. Gordon, J. A. Pople and M. J. Frisch, *J. Phys. Chem.*, 1992, **96**, 135–149.
51 M. J. Frisch, G. W. Trucks, H. B. Schlegel, G. E. Scuseria, M. A. Robb, J. R. Cheeseman, J. A. Montgomery Jr, T. Vreven, K. N. Kudin, J. C. Burant, J. M. Millam, S. S. Iyengar, J. Tomasi, V. Barone, B. Mennucci, M. Cossi, G. Scalmani, N. Rega, G. A. Petersson, H. Nakatsuji, M. Hada, M. Ehara, K. Toyota, R. Fukuda, J. Hasegawa, M. Ishida, T. Nakajima, Y. Honda, O. Kitao, H. Nakai, M. Klene, X. Li, J. E. Knox, H. P. Hratchian, J. B. Cross, C. Adamo, J. Jaramillo, R. Gomperts, R. E. Stratmann, O. Yazyev, P. Salvador, J. J. A. J. Austin, R. Cammi, C. Pomelli, J. W. Ochterski, P. Y. Ayala, K. Morokuma, G. A. Voth, P. S. Dannenberg, V. G. Zakrzewski, S. Dapprich, A. D. Daniels, M. C. Strain, O. Farkas, D. K. Malick, A. D. Rabuck, K. Raghavachari, J. B. Foresman, J. V. Ortiz, Q. Cui, A. G. Baboul, S. Clifford, J. Cioslowski, B. B. Stefanov, G. Liu, A. Liashenko, P. Piskorz, I. Komaromi, R. L. Martin, D. J. Fox, T. Keith, M. A. Al-Laham, C. Y. Peng, A. Nanayakkara, M. Challacombe, P. M. W. Gill, B. Johnson, W. Chen, M. W. Wong, C. Gonzalez and J. A. Pople, *GAUSSIAN 03 (Revision B.05)*, Gaussian, Inc., Pittsburgh, PA, 2003.
52 J. L. Brédas, R. Silbey, D. S. Boudreaux and R. R. Chance, *J. Am. Chem. Soc.*, 1983, **105**, 6555–6559.
53 J. Lee, J.-I. Lee, K.-I. Song, S.-J. Lee and H. Y. Chu, *Appl. Phys. Lett.*, 2008, **92**, 133304.
54 J. Lee, N. Chopra, S. H. Eom, Y. Zheng, J. Xue, F. So and J. Shi, *Appl. Phys. Lett.*, 2008, **93**, 123306.
55 V. Promaraka and S. Ruchirawat, *Tetrahedron*, 2007, **63**, 1602–1609.

